International Journal of Chemical, Materials and Biomolecular Sciences
ISSN: 2415-6620
Vol:12, No:5, 2018

Synthesis and Characterization of Nickel and Sulphur Sensitized Zinc Oxide Structures

Ella C. Linganiso, Bonex W. Mwakikunga, Trilock Singh, Sanjay Mathur, Odireleng M. Ntwaeaborwa

***Abstract*—**The use of nanostructured semiconducting material to catalyze degradation of environmental pollutants still receives much attention to date. One of the desired characteristics for pollutant degradation under ultra-violet visible light is the materials with extended carrier charge separation that allows for electronic transfer between the catalyst and the pollutants. In this work, zinc oxide n-type semiconductor vertically aligned structures were fabricated on silicon (100) substrates using the chemical bath deposition method. The as-synthesized structures were treated with nickel and sulphur. X-ray diffraction, scanning electron microscopy, energy dispersive X-ray spectroscopy were used to characterize the phase purity, structural dimensions and elemental composition of the obtained structures respectively. Photoluminescence emission measurements showed a decrease in both the near band edge emission as well as the defect band emission upon addition of nickel and sulphur with different concentrations. This was attributed to increased charger-carrier-separation due to the presence of Ni-S material on ZnO surface, which is linked to improved charge transfer during photocatalytic reactions.

***Keywords*—**Carrier-charge-separation, nickel, sulphur, zinc oxide, photoluminescence.

I. Introduction

ZINC oxide (ZnO) is one of the widely researched materials for a number of applications related to its renowned properties such as a direct wide band gap of 3.37 eV (at room temperature), high excitonic binding energy of 60 MeV, good mechanical strength, thermal, and chemical stability. [1]-[3]. One-dimensional nanostructures of ZnO have received much attention due to the high surface-to-volume ratio, direct carrier conduction path and high crystalline nature. Even though these properties are important in terms of application, some challenges when applying ZnO have been encountered such as photocorrosion under ultraviolet light, which is related to reducing photocatalytic activity during photocatalysic degradation of environmental pollutants experiments. Fabrication of heterostructures of ZnO could be a solution to obtaining materials with suitable properties for certain desired applications [4]. This is accomplished through interaction of the foreign material with the ZnO material, which results in novel properties and applications.

Nickel sulphides (Ni_xS_y) decorated on metal oxides are being researched for possible replacement of the normally used noble metals like Pt in dye-sensitized solar cells [5]. They are also being studied for application as co-catalysts in low cost visible light driven noble metal free photocatalysis of hydrogen production [6]. Ni_xS_y has also been applied in a number of heterogeneous catalysis reactions due to their good catalytic activity [7]. These materials have been chosen in this study since they are low cost, with the most stable phase Ni_3S_2 occurring naturally as a mineral (heazlelwoodite). In this paper, we report growth and characterization of Ni-S sensitized ZnO and discuss their possible application as photocatalysts.

II. Experimental Methods

The growth of ZnO/Ni-S heterostructures involved three steps. The first step was the growth of ZnO seed layer on silicon (Si) substrate by spin coating technique. An ethanol solution containing 0.5 M zinc acetate was spin coated on a pre-cleaned Si (100) substrate at 200 rpm for 30 seconds. The spin coated sample was oven dried at 250 ^oC in order to decompose zinc acetate and form ZnO nanoparticle-based seed layer. To increase the dispersion of ZnO nanoparticles on the Si substrate, the spin coating-to-drying process was repeated on the same substrate two more times. The second step was the growth of ZnO nanorods (NRs) on the seeded Si substrate by chemical bath deposition (CBD) method. The ZnO seeded substrates were placed vertically onto a bath containing a mixture of zinc nitrate hexahydrate ($Zn(NO_3)_2$. $6H_20$, 99.9%) and hexamethylene tetramine (HMT, $C_6H_{12}N_4$, 99.9%) equimolar solutions in distilled water. HMT was used as a complexing agent via ammonia formation to produce OH^- according to (1)-(4) [8]:

$$C_6H_{12}N_4 + 6H_2O \rightarrow 6HCHO + 4NH_3 \quad (1)$$

$$NH_3 + H_2O \rightarrow NH_4^+ + OH^- \quad (2)$$

$$Zn^{2+} + 2OH^- \rightarrow Zn(OH)_2 \quad (3)$$

$$Zn(OH)_2 \rightarrow ZnO + H_2O \quad (4)$$

The bath was maintained at 93 ^oC for 3 hours. The samples were then removed from the bath, washed with distilled water

E. C. Linganiso is with the Molecular Sciences Institute, School of Chemistry, and Microscopy and microanalysis Unit, University of the Witwatersrand, Johannesburg, Private Bag 1, 2050 SA (corresponding author, phone: +27 11 717 1333; e-mail: cebisa.linganiso@wits.ac.za).

B. W. Mwakikunga is with the Council for Scientific and Industrial Research, Pretoria, P O Box 395, 0001 SA.

T. Singh is with the Department of Chemistry at the University of Cologne, Cologne, 50939 Germany.

S Mathur is with the Institute of Inorganic and Materials Chemistry at the University of Cologne, Cologne, 50939 Germany.

O. M. Ntwaeaborwa is with the School of Physics, University of the Witwatersrand, Private Bag 1, 2050 SA (corresponding author, phone: +27 11 717 6887; martin.ntwaeaborwa@wits.ac.za).

and ethanol and dried in air. The samples were further dried in oven at 100 °C for 1 hour to evaporate the solvent. The third step involved deposition of nickel (Ni) and sulphur (S) on the ZnO surface. The as-grown ZnO films were immersed on a bath containing 0.01 M nickel chloride in 0.01 M HMT solution and 0.03 M sodium sulphide solution in water. The bath temperature was kept at 80 °C for 30, 45, and 60-minute intervals in order to achieve varying Ni-S concentration on the ZnO surface. The samples were then washed thoroughly using distilled water and ethanol and oven dried at 100 °C for 1 hour.

The prepared samples were characterized for phase composition using a Bruker D8 Advanced powder X-ray diffractometer (XRD) with Cu Kα radiation wavelength of 0.154 nm X-ray. Morphology distribution was analyzed using a JEOL JSM-7800 field emission scanning electron microscope (FE-SEM) coupled with Oxford Aztec 350 X-Max80 energy-dispersive X-ray spectroscopy (EDS). The EDS was used to determine the elemental composition analysis of the prepared structures. Photoluminescence (PL) emission measurements were recorded using a PL system consisting of a 325-nm He-Cd laser excitation source.

III. Results

A. Figures and Tables

XRD pattern of the as-prepared ZnO nano-arrays (ZNA-prep) as well as those immersed in Ni-S solution at different times (ZnA-30min, ZnA-45 min and ZnA-60min) are shown in Fig. 1. All scans were in good agreement with ZnO hexagonal wurtzite crystallite structure with a prominent peak being the (002) orientation indicating a high degree of anisotropic growth of ZnO structures along the *c*-axis. No additional peaks were detected after the addition of Ni-S onto the ZnO structures. This can be attributed to a low degree crystallinity of the Ni-S phases that were added to the ZnO structures.

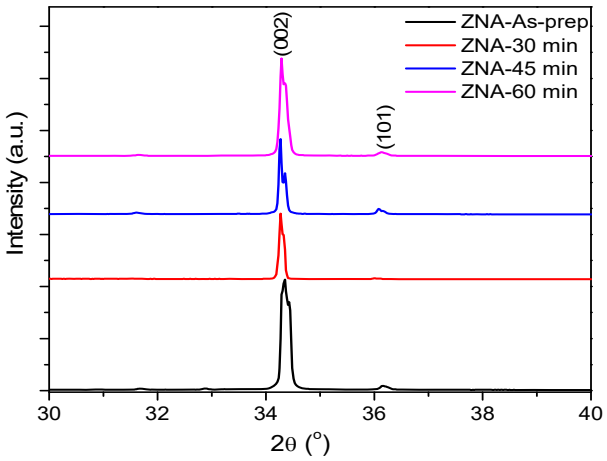

Fig. 1 XRD profile for the prepared ZnO and ZnO coated with Ni-S

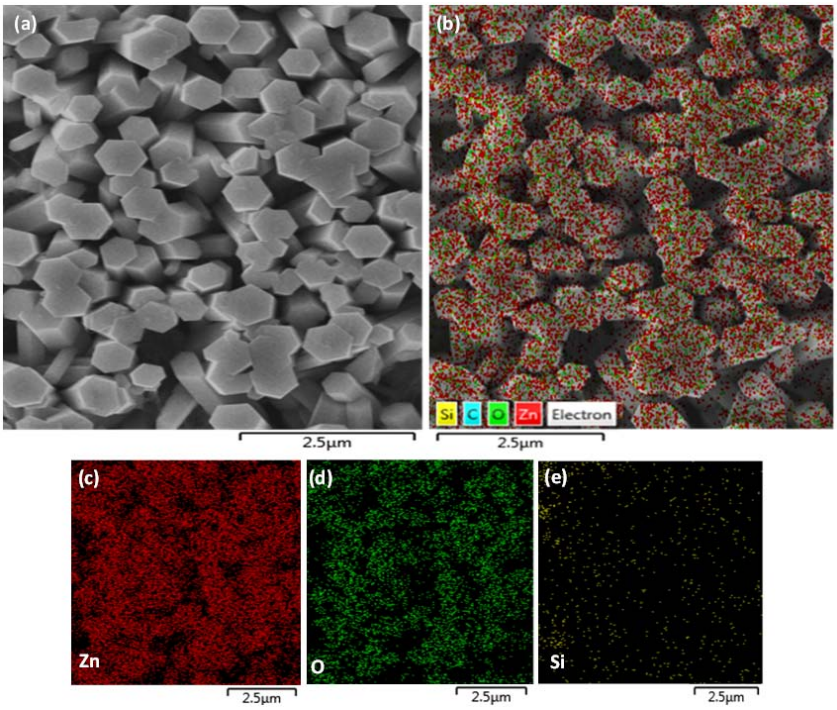

Fig. 2 SEM image (a) and EDS mapped images (b-e) for ZnO thin film

Fig. 2 shows the SEM image (a) and mapped EDS images (b-e) of the as-prepared ZNA structures from the top side of the thin film. It can be seen that the structures are vertically aligned and closely packed on the Si(100) surface. From the

top of the structures, it was observed that every single rod had taken hexagonal shape, which is common with ZnO NRs. The average diameter distribution of the structures was measured to be approximately 230 nm and their height was measured to be approximately 1.6 microns. The mapped images confirmed the presence of the dominant zinc, oxygen, and silicon elements, which made up the overall structure. The presence of Si can be attributed to the diffusion of Si/SiO_2 to the ZnO structure from the substrate surface during the growth process.

Fig. 3 shows the SEM image and EDS for the ZnA immersed in Ni-S for 45 minutes. In order to prevent/reduce the charging effect during SEM imaging, the sample was coated with a thin layer of gold-palladium (Au-Pd) nanoparticles. No obvious added crystal structure was observed in the SEM image because of Ni-S material addition. The EDS analysis however, showed the presence of zinc, oxygen, silicon, nickel and sulphur, which confirmed their presence in the films.

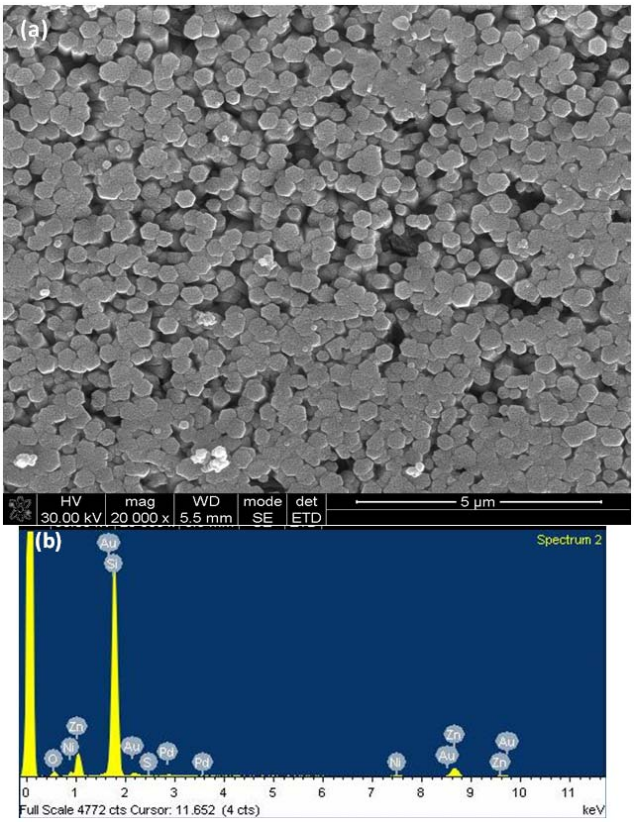

Fig. 3 SEM image (a) and EDS (b) for the ZnO coated with Ni-S for 45 minutes

Fig. 4 (a) shows the room temperature PL spectra of bare ZnO structures and ZnO structures coated with different concentrations of Ni-S, measured at an excitation wavelength of 325 nm using He-Cd laser. The high excitation energy allows for the excitation of electrons from the valence band (VB) to the conduction band (CB) as well as deep levels within the band gap of the ZnO. The PL spectra of all the samples exhibited two emission bands; the UV and the broad visible bands located at about 380 nm and (450-800 nm) range respectively. There were no new visible luminescence peaks observed due to the additional Ni-S material in the presented range. The UV emission represents the near band-edge (NBE) emission of ZnO, which is due to the radiative recombination of free excitons through exciton-exciton collision process. The second emission peak covers a large part of the visible spectrum from blue to red region (450-800 nm) with a maximum in the orange region (approximately 590 nm). This band is associated with deep level defects in the ZnO material.

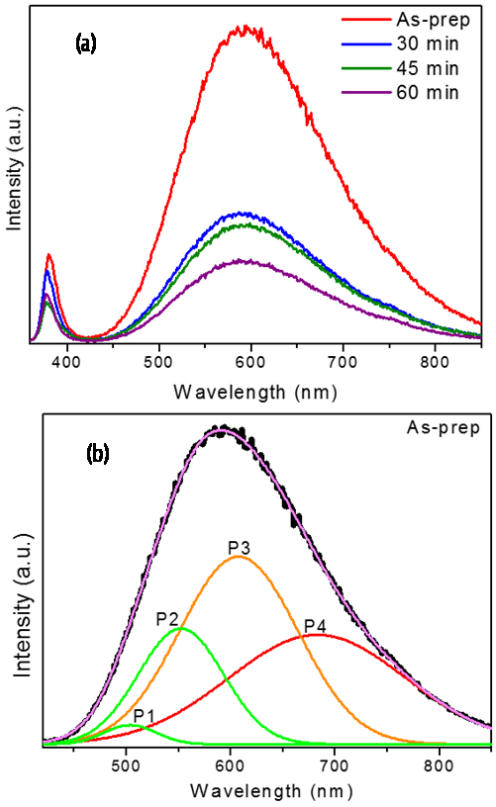

Fig. 4 Photoluminescence of the prepared samples (a) and deconvoluted defect band (b) for the as-prepared ZnO structures

The Gaussian deconvolution of the visible range emission peak of bare ZnO structures is shown in Fig. 4 (b). Four bands were produced from the peak appearing at 503, 552, 607, and 682 nm. These bands together with the UV band emission are listed with their possible assignments in Table I. The green emission band observed at 503 nm has been attributed to recombination of electrons in the singly ionized oxygen vacancies (V^{+}_{o}) with photo-excited holes in the valence band [9]. The second green emission band located at 552 nm has been attributed to recombination of CB electrons with deeply trapped, double charged oxygen vacancy (V_{o}^{++}) holes [10]. The orange emission band located at 607 nm is the most intense of all the emission bands and has had many suggested origins. A recent study proposed that a transition from an oxygen vacancy (V_o) to zinc interstitial sites (Zn_i) occurs

which is a result of a rearrangement of intrinsic defects after growth of the material [11]. These sites have been reported to favor the photo-catalytic decomposition of dyes due to their supposed role as charge carrier traps, which prolong the lifetime of a photo-generated hole or electron [11]. This improves the ability of the material to catalyze photo-induced chemical reactions. The red emission band located at 682 nm is less popular and it has been linked to excess oxygen in the ZnO material. This band has been attributed to a transition of electron from CB to oxygen interstitials that are located about 1.82 eV below CB [12]. It is worth noting though that the exact location of these defect centers is not conclusively established [13].

The same excitation wavelength of 325 nm was used for all the ZnO/Ni-S structures. A weak luminescence emission was observed at both the NBE emission and the visible emission bands when compared to the bare ZnO structures. The suppression of the ZnO emission suggests that the Ni-S materials on ZnO surface capture the photo-induced electrons prolonging the separation of photo-induced electrons and holes. This is a desired attribute for materials to have high photocatalytic activity. Another possible contributor to the defect band quenching effect could be a nonradiative recombination at the defect sites in the ZnO/Ni-S interfaces [6].

TABLE I
ASSIGNMENT OF THE ZNO EMISSION BANDS OBTAINED FROM THE PL

Wavelength (nm)	Energy (eV)	Assignment
380	3.26	NBE
503 (P1)	2.46	V^{+}_{o} to VB
552 (P2)	2.25	CB to V_{o}^{++}
607 (P3)	2.04	V_{o} to Zn_{i}
682 (P4)	1.82	CB to O_{i}

IV. CONCLUSION

Vertically aligned ZnO and Ni-S sensitized ZnO structures were fabricated using the CBD method. The hexagonal wurtzite phase of ZnO and its hexagonal shaped rod-like structures were confirmed using XRD and SEM analysis, respectively. Elemental analysis confirmed that the devices consisted of all the desired intended elements. The prolonged photo-induced charge-carrier-separation was achieved through the introduction of Ni-S material on ZnO surface. This was evidenced by reduced ZnO PL emission intensity upon Ni-S introduction. The synthesized structures are candidates for application in visible light assisted catalysis of pollutant degradation chemical reactions, which form part of our future goals.

ACKNOWLEDGMENT

The authors would like to acknowledge the National Research Foundation of South Africa for supporting the research and presentation of this work.

REFERENCES

[1] Q. Zhou, J. Z. Wen, P. Zhao, W. A. Anderson, "Synthesis of Vertically-Aligned Zinc Oxide nanowires and Their Application as a Photocatalyst" *Nanomaterials* vol. 7 pp. 1-13, January 2017.

[2] S. Dhara, P. K. Giri, "ZnO Nanowire Heterostructures: Intriguing Photophysics and Emerging Applications" *Rev. Nanosci. Nanotechnol.* vol. 2 pp. 1-24, March 2013.

[3] A. Syed, M. Kalloudis, V. Koutsos, E. Mastropaolo, "Controlled hydrothermal growth of vertically-aligned zinc oxide nanowires using silicon and polymide substrates" *Microelectronic Engineering* vol. 145 pp. 86-90, September 2015.

[4] A. Bera, D. Basak, "Photoluminescence and photoconductivity of ZnS-coated ZnO nanowires" *ACS Appl. Mater. Interfaces* vol. 2 pp. 408-412, January 2009.

[5] W. S. Chi, J. W. Han, S. Yang, D. K. Roh, H. Lee, J. H. Kim, "Employing electrostatic self-assembly of tailored nickel sulphide nanoparticles for quasi-solid-state dye-sensitized solar cells with Pt-free counter electrodes" *Chem. Commun.* vol. 48 pp 9501-9503 August 2012.

[6] J. Zhang, S. Z. Qiao, L. Qi, J. Yu, "Fabrication of NiS modified CdS nanorod p-n junction photocatalysts with enhanced visible-light photocatalytic H2-production activity" *Phys. Chem. Chem. Phys.* vol. 15 pp. 12088-12094, April 2013.

[7] C.-H. Lai, M.-Y. Lu, L.-J. Chen, "Metal sulfide nanostructures: synthesis, properties and applications in energy conversion and storage" *J. Mater. Chem.* vol. 22 pp. 19-30, November 2011.

[8] B.-R. Huang, J.-C. Lin, "A facile synthesis of ZnO nanotubes and their hydrogen sensing properties" *Appl. Surf. Sci.* vol. 280 pp. 945-949, September 2013.

[9] K. Vanheusden, C. H. Seager, W. L. Waren, D. R. Tallant, J. A. Voigt, "Correlation between photoluminescence and oxygen vacancies in ZnO phosphors" *Appl. Phys. Lett.* vol. 68 pp. 403-405, January 1996.

[10] D Liu, Y. Lv, M. Zhang, Y. Liu, Y. Zhu, R. Zong, Y. Zhu, "Defect-related photoluminescence and photocatalytic properties of porous ZnO nanosheets" *J. Mater. Chem. A* vol. 2 pp. 15377-15388, July 2014.

[11] J. Kegel, F. Laffir, I. M. Povey, M. E. Pemble, "Defect-promoted photo-electrochemical performance enhancement of orange-luminescent ZnO nanorod-arrays" *Phys. Chem. Chem. Phys.* vol. 19 pp. 12255-12268, April 2017.

[12] R. Raji, K. G. Gopchandran, "ZnO nanostructures with tunable visible luminescence: Effects of linetikc of chemical reduction and annealing" *J. Sci. Adv. Mater. Devices* vol. 2 pp. 51-58, March 2017.

[13] K. Bandopadhyay, J. Mitra, "Zn interstitials and O vacancies responsible for n-type ZnO: what do the emission spectra reveal?" *RSC Adv.* vol. 5 pp. 23540-23547, February 2015.